REMARKS/ARGUMENTS

Favorable reconsideration of this application as presently amended and in light of the following discussion is respectfully requested.

Claims 1-3 and 7-17 are presently active; Claim 4 was previously cancelled without prejudice or disclaimer, Claims 5 and 6 have been presently cancelled without prejudice or disclaimer, Claim 1 has been presently amended. New Claims 15-17 have been added. No new matter has been added.

In the Office Action, Claims 5 and 6 were rejected under 35 U.S.C. 112, second paragraph, as being indefinite. Claims 1-3, 5-12 and 14 were rejected under 35 U.S.C. 103(a) as being unpatentable over Aoyama et al (U.S. Patent No. 5,651,827) in view of Shamouilian et al (U.S. Patent No. 6,440,221) and Nath (U.S. Patent No. 4,149,086), Claim 13 was rejected under 35 U.S.C. 103(a) as being unpatentable over Aoyama et al in view of Shamouilian et al and Nath as applied to Claims 1-3, 5-12, and 14 and further in view of Hillman (U.S. Patent No. 5,997,649).

Claim Summary: Claim 1 as clarified defines:

> A substrate processing apparatus, comprising:
> a processing vessel ***made of metal*** that defines a processing space;
> an ultraviolet light source that irradiates ultraviolet light into the processing vessel;
> a gas injection nozzle unit that is connected to a side of the processing vessel and is configured to inject gas into the processing vessel;
> an opaque case made of quartz that covers an inner wall of the processing vessel and includes an opening arranged to face against the ultraviolet light source through which opening the ultraviolet light passes;
> a remote plasma part that is connected to the side of the processing vessel at which the gas injection nozzle unit is arranged and is configured to supply radicals to the processing vessel ***through a supply line***;
> a heater portion that heats a substrate introduced inside the opaque case to a predetermined temperature;
> a holding member that holds the substrate above the heater portion; and
> rotational drive means for rotating an axis of the holding member that penetrates through the heater portion. [Emphasis added.]

Regarding amended Claim 1, support for the phrase "made of metal" added to Claim 1 is found on page 65, line 23, in the specification and support for the phrase "through a supply line" added to Claim 1 is found on page 31, lines 22-28, in the specification. Thus, no new matter has been added.

Regarding the 35 U.S.C. 112, second paragraph, rejection to Claims 5 and 6, these claims have been replaced with new Claims 16 and 17. Further, the subject matter of original Claim 4 has been included in new Claim 15 to provide an antecedent basis for "the transparent case." Thus, the 35 U.S.C. 112, second paragraph, rejection has been overcome.

The art deficiencies:

The asserted combination of Aoyama, Shamouilian and Nath does not disclose or suggests all of the elements of independent Claim 1, for at least the following reasons.

None of Aoyama, Shamouilian and Nath individually or in combination discloses, as recited in Claim 1, (1) an "opaque case made of quartz that covers an inner wall of the processing vessel" (hereinafter the opaque case feature), and (2) a "remote plasma part configured to supply radicals to the processing vessel through a supply line" (hereinafter the remote plasma part feature).

The opaque case feature: Regarding the opaque case feature, the originally filed specification describes by way of illustration on page 65, lines 20-26, that opaque case 102, 104, 106, 108 can be arranged in order to protect the processing vessel 22 made of aluminum alloy from gas and ultraviolet light as well as to prevent metal contamination of the

processing space 84 by the processing vessel 22. Applicant's substrate processing apparatus can thus utilize an opaque case that covers an inner wall of the processing vessel in order to protect the processing vessel from ultraviolet light. The specification illustrates this effect with regard to ultraviolet light (which the opaque case protects against) having a wavelength of 172 nm. See specification on page 23, lines 5-6. Ultraviolet light of this type is generally called UVC (with a wavelength below 280 nm). Other ultraviolet light sources are known. Nath describes the use of UVA with a wavelength of 315 to 400 nm. UVC oxidizes metal to a greater degree than UVA.

Thus, the substrate processing apparatus of Claim 1 which includes an opaque case can protect a processing vessel (e.g., a processing vessel made of an aluminum alloy) from gas and ultraviolet light (e.g., UVA or UVC) as well as to prevent metal contamination of the processing space by the processing vessel.

The Office Action asserted on page 3 that Aoyama teaches "an opaque case (liner)." The Office Action cites the Abstract and col. 3, lines 35-64. However, Aoyama merely describes a translucent or opaque reactor vessel 1, and an external heater 30 or an internal heater 30a. Figure 9 of Aoyama is reproduced below.

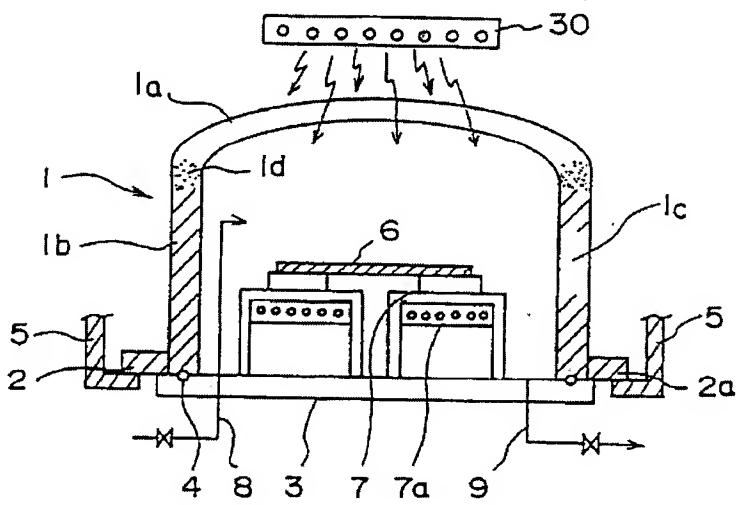

Fig. 9

Thus, Aoyama fails to disclose or suggest an opaque case made of quartz ***that covers an inner wall of the processing vessel***, as defined in Claim 1. Indeed, element 1 in Aoyama is the inner wall of the processing vessel.

The Office Action applied Shamouilian for an asserted teaching of a PECVD chamber with a gas supply provided at all flour walls. See page 3 of the Office Action. Shamouilian describes that the materials used to fabricate the process chamber 25 include metals, ceramics, glasses, polymers, etc. Yet, Shamouilian fails to disclose or suggest an opaque case made of quartz that covers an inner wall of the processing vessel, as defined in Claim 1. Thus, the deficiencies in Aoyama regarding the opaque case feature are not overcome by Shamouilian.

The Office Action applied Nath for an asserted teaching of tungsten lamps as a source of UV. Nath is directed to a dentistry irradiation device. Nath fails to disclose or suggest an opaque case made of quartz that covers an inner wall of the processing vessel, as defined in Claim 1. Thus, the deficiencies in Aoyama regarding the opaque case feature are not overcome by Nath.

The remote plasma part feature: Regarding the remote plasma part feature, the Office Action asserted that Shamouilian teaches that a RF power source, electrode, and an antenna 125 act as plasma generators. The Office Action on page 2 asserted that col. 4, lines 35-67, taught "remote plasma parts." Yet, lines 35-51 describe an electrostatic chucking device and lines 52-67 describe an inductively coupled plasma system. As seen in Figure 4 of Shamouilian, the plasma generated under the rf coils in the processing space would be directly over the substrate to be processed. In other words, Shamouilian describes that the plasma generators generate a plasma of the process gas within the process chamber 25.

Further, it is well known in the art that the term "remote plasma" means generating a plasma (radicals) in a remote place and supplying the plasma from the remote place to a processing vessel through a supply line. As evidence, this knowledge in the art, the examiner's attention is directed to the attached article for the Journal of Vacuum Science and Technology (1993).

Accordingly, it has not been made clear where (in this complex reference) that Shamouilian describes a remote plasma part. 37 C.F.R. § 104 (c)(2) indicates that, when a reference is complex or shows or describes inventions other than that claimed by the applicant, the particular part relied on must be designated as nearly as practicable. Accordingly, the requirement under 37 C.F.R. § 104 (c)(2) has not been met, and can not be met with Shamouilian.

Thus, Shamouilian does not teach or suggest a remote plasma part that is connected to the side of the processing vessel, as recited in Claim 1.

Conclusion: For at least the foregoing reasons, the asserted combination of Aoyama, Shamouilian and Nath does not disclose or suggests all of the elements of independent Claim 1, and withdrawal of the rejection from the application is respectfully requested.

Hence, when the defined features are considered as a whole, Claim 1 and the claims dependent therefrom are believed to patentably define over the art of record.

In view of the present amendment and in light of the above discussions, the outstanding grounds for rejection are believed to have been overcome. The application as amended herewith is believed to be in condition for formal allowance. An early and favorable action to that effect is respectfully requested.

Respectfully submitted,

OBLON, SPIVAK, McCLELLAND,
MAIER & NEUSTADT, P.C.

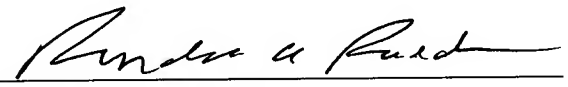

Steven P. Weihrouch
Attorney of Record
Registration No. 32,829

Ronald A. Rudder, Ph.D.
Registration No. 45,618

Customer Number
22850

Tel: (703) 413-3000
Fax: (703) 413 -2220
(OSMMN 08/07)

Attachment: Article from the Journal of Vacuum Science and Technology (1993)

I:\ATTY\RAR\AMENDMENTS(2007)\268669US\RESPONSE DUE 12-11-08.DOC

ATTACHMENT

Remote plasma etching reactors: Modeling and experiment

Shashank C. Deshmukh and Demetre J. Economou[a)]
Department of Chemical Engineering and Texas Center for Superconductivity, University of Houston, Houston, Texas 77204-4792

(Received 23 June 1992; accepted 14 December 1992)

A combined theoretical–experimental analysis of a remote plasma etching reactor was undertaken. Chlorine plasma etching of polysilicon was chosen as a case study to illustrate the approach. A model of the plasma (radical source) and of the transport and reaction of radicals through the downstream section was developed. The effect of tube dimensions, gas pressure, flow rate, and wall recombination probability was examined. In the parameter range investigated, low pressure, high flow rate, short downstream section, and low wall recombination probability favor higher radical fluxes at the substrate. A conflict arises in choosing the tube radius. A tubular reactor with different radii for the source and downstream sections is proposed to optimize the radical flux. Model predictions were tested in a radical beam reactor. Actinometry was used to monitor the Cl-atom density in the source and to verify the predictions of the plasma model. Using the wall recombination probability as the only adjustable parameter, reasonable agreement between predicted and measured atom flux at the reactor exit was also obtained.

I. INTRODUCTION

Remote plasma processing is finding increasing applications in the etching and deposition of damage-free thin films. This technique differs from *in situ* plasma processing in that the substrate on which etching or deposition takes place is not exposed to the harsh plasma environment. Thus, bombardment of the substrate by ions as well as ultraviolet (UV) photons and soft x rays is minimized or totally eliminated. The result is reduced radiation damage and increased device yield. In a typical remote plasma processing reactor, radicals are generated in a discharge sustained at 13.56 MHz (radio frequency) or 2.45 GHz (microwave frequency) at a location upstream from the substrate. The radicals are then transported to the processing chamber where etching or deposition takes place. Applications include *in situ* deposition of thin film superconductors using O atoms,[1] native oxide removal at low temperature using hydrogen atoms,[2] deposition of GaN passivation films using N atoms, deposition of Si and its compounds,[3] etching of polymers using atomic oxygen,[4] and etching of various compound semiconductors[5] and $YBa_2Cu_3O_{6+x}$ thin films using chlorine atoms.[6]

In many remote plasma processing applications, one is interested in achieving high degree of gas dissociation in the plasma and minimal radical loss in the downstream section, so as to maximize the radical flux at the substrate. Proper selection of reactor dimensions and operating conditions to achieve this goal is difficult based on intuition alone. Mathematical models tested with experimental measurements are valuable for reactor design, process optimization, and development of process control strategies.

In a previous work,[7] a model was developed to investigate the factors which affect the radical density in the plasma (radical source model). The model considered a discharge of length L_p (Fig. 1) sustained in a cylindrical quartz tube of radius R. Rate coefficients for electron–particle reactions in the Cl_2/Cl mixture were obtained by solving the Boltzmann transport equation for the electron energy distribution function. These rate coefficients were parametrized and used in a plasma model to calculate the self-sustaining electric field, electron density, and atomic chlorine density in the plasma. For otherwise identical conditions, nearly the same atom density was obtained in 13.56 MHz and 2.45 GHz discharges. It was found that very high degrees of molecular dissociation are possible with only a few watts per cubic centimeter in the plasma. Despite the fact that the atom density decreased with increasing feed gas flow rate, the atom flux increased with flow rate. In the parameter range investigated, lower pressures and larger tube radii favored higher atom density in the plasma. Wall recombination was not an important sink for Cl atoms as long as the wall recombination reaction probability was less than 10^{-4}.

In this article, an extension of the previous model is reported including transport and reaction in the downstream section. Factors which influence the radical flux at the reactor exit (i.e., at the substrate) are studied. In addition, an experimental system is used to test the predictions of the radical source model[7] and of the overall reactor model. More detailed models of remote plasma deposition[8] and etching[9] reactors have been reported recently. However, these models are computationally more difficult and require substantial CPU time. The goal of the present work is to provide a model which is detailed enough yet it can be executed in a short CPU time. Such models are important for model-based process control of plasma etching and deposition.

II. MATHEMATICAL MODEL

The overall reactor model was divided into two parts: plasma (radical source) and downstream sections (Fig. 1). Separate models were written for the two sections. These models were coupled at the interface between the sections. The modeling approach is shown in Fig. 2. First, the Boltz-

a)Author to whom all correspondence should be addressed.

 0734-211X/93/020206-10$01.00

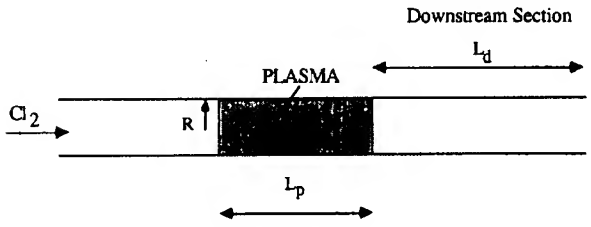

FIG. 1. Schematic of a tubular reactor in which an electrodeless chlorine discharge is sustained.

mann equation was solved for a set of values of E/N, ω/N, and gas composition in the parameter range of interest. Here E is electric field, N is total gas density, and ω is plasma excitation frequency. The electron transport properties (e.g., mobility and diffusivity) and rate coefficients of reactions involving electrons were thus obtained from the electron energy distribution function (eedf). These quantities were parametrized and used in the radical source model. The latter consisted of mass and energy conservation equations to determine the self-sustaining electric field, electron density, and atomic chlorine density in the plasma. Inputs to the radical source model included gas density, flow rate, power, plasma radius and volume, and excitation frequency. The only adjustable parameter of the model was the wall recombination probability of the radicals, γ_p. The atomic chlorine density obtained by the radical source model was used as a boundary condition at the inlet of the downstream section. Again, the only adjustable parameter of the downstream model was the wall recombination probability of the radicals, γ_d. The final result was the radical density and flux at the tube exit.

A. Radical source model

This model was described in detail in Ref. 7. Hence, only a brief description is given here.

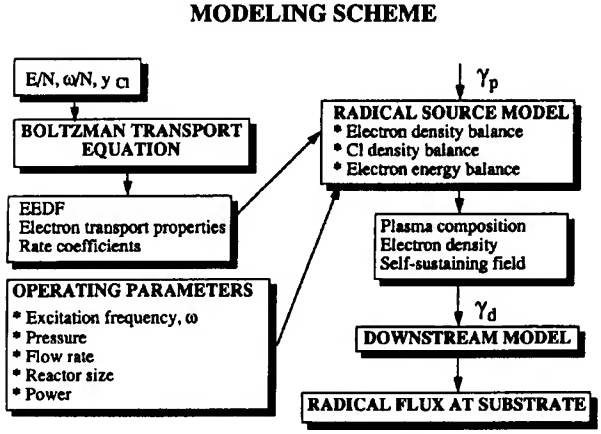

FIG. 2. Overview of the modeling approach.

1. Electron transport and reaction coefficients

These were found by solving the Boltzmann equation for the eedf. Since complete dissociation can be achieved readily in a chlorine plasma, it is important to include the effect of Cl atoms on electron and plasma kinetics. At a frequency of 2.45 GHz, the eedf cannot follow the rapid variations of the field. Hence, a time-average distribution can be used.

Cross sections for various elastic and inelastic processes for atomic and molecular chlorine were taken from Rogoff *et al.*[10] and Aydil and Economou.[11] Inelastic processes for molecular chlorine included vibrational excitation, ionization, dissociative attachment, and excitation to $B\,^3\Pi$, $2\,^1\Pi$, $2\,^1\Sigma$, and $C\,^1\Pi$ states. Excitation to the $C\,^1\Pi$ state is dissociative and is the main channel producing atomic chlorine. Inelastic processes for atomic chlorine included ionization and excitation to six different electronic states. Table I shows the electron and neutral particle reactions. A computer code developed by Luft[12] was used to solve the Boltzmann equation. For given ratio of excitation frequency to neutral gas density, ω/N, the rate coefficients for various electron particle reactions, k_j, were parametrized as functions of E/N and y_{Cl} (mole fraction of atomic chlorine in the discharge), and were used in the balance equations shown below.

The plasma model yields three key plasma properties, namely, the self-sustaining electric field, the electron density, and the atomic chlorine density. In order to determine these properties, three independent equations are required. These are the electron density balance, the Cl density balance and the power balance.

2. Electron density balance

The electron density balance can be written as

$$\frac{d}{dt}n_e = k_{i1}y_{Cl}Nn_e + k_{i2}(1-y_{Cl}) \times Nn_e - k_a(1-y_{Cl})Nn_e - \frac{D_{ae}}{\Lambda^2}n_e. \quad (1)$$

Here k_{i1}, k_{i2}, and k_a are the rate coefficients for atomic ionization, molecular ionization, and attachment, respectively. D_{ae} is the ambipolar diffusivity, Λ is the electron diffusion length, and n_e is the electron density. The terms on the right-hand side (rhs) represent ionization of atomic chlorine, ionization of molecular chlorine, attachment to molecular chlorine, and diffusion to the walls of the container, respectively. Electron diffusion losses were evaluated as before.[7] Since the electron density is not modulated in time under the microwave field, the left-hand side (lhs) of Eq. (1) is equal to zero.

3. Atomic chlorine density balance

If Q_0 is the feed rate of molecular chlorine (sccm) then the component balance for atomic chlorine can be written as

TABLE I. Important reactions in the chlorine discharge.

Reaction		Threshold (eV)
Molecular ionization	$Cl_2+e^- \rightarrow Cl_2^+ +2e^-$	11.5
Atomic ionization	$Cl+e^- \rightarrow Cl^+ +2e^-$	13.0
Dissociative attachment	$Cl_2+e^- \rightarrow Cl_2^{-*} \rightarrow Cl+Cl^-$	
Dissociative excitation	$Cl_2+e^- \rightarrow Cl_2^*(C\,^1\Pi) + e^- \rightarrow 2Cl+e^-$	3.12
Dissociative ionization	$Cl_2+e^- \rightarrow Cl^+ +Cl+2e^-$	11.5
Electronic excitation	$Cl_2+e^- \rightarrow Cl_2^*(B\,^3\Pi) + e^-$	2.50
(Molecular chlorine)	$Cl_2+e^- \rightarrow Cl_2^*(2\,^1\Pi \& \; 2\,^1\Sigma) + e^-$	9.25
Vibrational excitation	$Cl_2+e^- \rightarrow Cl:::Cl^*+e^-$	0.069
Electronic excitations (six) (Atomic chlorine)	$Cl+e^- \rightarrow Cl^*+e^-$	
Ion–ion recombination	$Cl_2^+ +Cl^- \rightarrow Cl_2+Cl$	
	$Cl^+ +Cl^- \rightarrow 2Cl$	
Volume recombination	$Cl+Cl+M \rightarrow Cl_2+M$	
Wall recombination	$Cl+\text{wall} \rightarrow 1/2Cl_2+\text{wall}$	

$$\frac{2\times 4.48\ 10^{17}Q_0}{V_p}\frac{y_{Cl}}{(2-y_{Cl})}=(k_a+2k_d)N(1-y_{Cl})n_e - 2k_vN^3y_{Cl}^2-2\frac{k_{sp}}{R}Ny_{Cl}, \quad (2)$$

where V_p is the plasma volume, k_d is the rate coefficient for electron-impact dissociation of molecular chlorine, and k_v is the rate coefficient for volume recombination of atomic chlorine. The factor $4.48\ 10^{17}$ converts sccm to molecules/s. The lhs of Eq. (2) is the rate at which atomic chlorine leaves the plasma volume. The first term on the rhs represents the rate of production of Cl by dissociative attachment and dissociation. The second and third terms on the rhs represent the loss rate of Cl by volume recombination and surface recombination on the walls of the discharge tube, respectively. The surface recombination rate coefficient, k_{sp}, is given by

$$k_{sp}=\frac{\gamma_p}{4}\left(\frac{8kT}{\pi M_{Cl}}\right)^{1/2}, \quad (3)$$

and γ_p is the reaction probability on the walls exposed to the plasma, k is the Boltzmann constant, M_{Cl} is the mass of atomic chlorine, and T is the gas temperature. The last term in Eq. (2) is multiplied by the surface-to-volume ratio ($=2/R$, where R is the tube radius), to transform the surface reaction into a volumetric term in the material balance. Equation (2) assumes a well-mixed plasma zone. This assumption is reasonable since the Peclet number [see Eq. (6)] calculated based on the plasma length L_p is around unity.

4. Power balance

The energy absorbed from the field by the electron cloud is lost to elastic and inelastic collisions with the gas particles. At steady state, the power balance can be written as

$$\frac{P}{V_p}=\sum_i\frac{2m}{M_i}\langle\epsilon\rangle k_{mi}n_eNy_i+\sum_i\epsilon_ik_i(1-y_{Cl})Nn_e + \sum_j\epsilon_jk_jy_{Cl}Nn_e+\langle\epsilon\rangle k_{i1}y_{Cl}Nn_e + \langle\epsilon\rangle k_{i2}(1-y_{Cl})Nn_e, \quad (4)$$

where P is the power input to the plasma, $\langle\epsilon\rangle$ is the average electron energy (averaged over the eedf), ϵ_i is the energy loss for the ith inelastic process for molecular chlorine, k_i is the corresponding rate coefficient; ϵ_j and k_j are the corresponding quantities for atomic chlorine. The first term on the rhs accounts for the rate at which energy is lost by the electrons through elastic collisions. The second and third terms on the rhs represent the rate at which energy is lost via inelastic processes involving molecular and atomic chlorine, respectively. Finally, the fourth and fifth terms represent the rate at which energy is needed to bring the electrons produced by ionization to the average electron energy.

B. Downstream section model

In the downstream section there is no source of atomic chlorine. However, atoms are lost by volume and surface recombination reactions. The atom density distribution is described by the convective–diffusion equation, which at steady state is written as

$$\frac{4}{(2-y_{Cl})^2}\frac{d}{d\zeta}y_{Cl}-\frac{2}{(2-y_{Cl})\mathrm{Pe}}\left[\frac{d^2}{d\zeta^2}y_{Cl} + \frac{1}{(2-y_{Cl})}\left(\frac{d}{d\zeta}y_{Cl}\right)^2\right]+\mathrm{Da}_vy_{Cl}^2+\mathrm{Da}_wy_{Cl}=0, \quad (5)$$

where

$$\zeta=\frac{x}{L_d}, \quad \mathrm{Pe}=\frac{4.48\times 10^{17}Q_0L_d}{ND_{AB}\pi R^2}, \quad (6)$$

$$\mathrm{Da}_v=\frac{2k_vN^3\pi R^2L_d}{4.48\times 10^{17}Q_0}, \quad \mathrm{Da}_w=\frac{2k_{sd}\pi RL_dN}{4.48\times 10^{17}Q_0}. \quad (7)$$

The boundary conditions are at

$$\zeta=0, \quad y_{Cl}=y_{Cl,0} \tag{8}$$

and at

$$\zeta=1, \quad \frac{d}{d\zeta}y_{Cl}=0, \tag{9}$$

where $y_{Cl,0}$ is the mole fraction of atomic chlorine at the exit from the plasma. This is the quantity that couples the source and downstream sections of the reactor. L_d is the length of the downstream section, ζ is dimensionless distance, and D_{AB} is the diffusivity of Cl in Cl_2. The first term in Eq. (5) represents convection by bulk gas flow, the second term is due to diffusion, and the third and fourth terms represent loss of atomic chlorine by volume and wall recombination, respectively. Equation (5) implies that radical concentration gradients along the tube radius are negligible compared to those along the tube axis. This assumption is justified for high aspect ratio tubes (large L_d/R) and slow wall recombination reactions. The Peclet number (Pe) shows the relative importance of convection (bulk gas flow) as compared to diffusion. It is the ratio of characteristic time for axial diffusion to a characteristic gas residence time. The Damköhler number (Da_v) shows the relative importance of volume recombination as compared to gas convection. It is the ratio of a characteristic gas residence time to a characteristic time for volume recombination. Da_w is similar to Da_v except that wall recombination replaces volume recombination. The ratio $Da_v/Da_w=Rk_vN^2/k_s$ shows the relative importance of volume recombination as compared to wall recombination. Note that volume recombination is enhanced by increasing N (pressure), and wall recombination is enhanced by increasing the surface to volume ratio (which is equal to $2/R$).

For the experimental conditions of this study at a feed flow rate of 6 sccm and 1 Torr pressure, the gas residence time in the downstream section of the tube is 282 ms; at 0.8 sccm and 0.25 Torr it is 529 ms. The Cl^+ and Cl_2^+ ions produced in the plasma are lost in the downstream section by diffusion to the walls and via ion–ion recombination with Cl^-. The average lifetime of these ions in the downstream section is estimated to be 3.5 ms at 1 Torr and 1 ms at 0.25 Torr. This is much less than the gas residence time in the downstream section. Electrons exiting the plasma zone cool down and are lost rapidly by attachment. Furthermore, the production of atomic chlorine by ion–ion recombination and electron attachment is insignificant due to the low concentration of charged species. As a result there is no need to include charged species chemistry in the downstream section. However, for short downstream sections, charged particle chemistry may be important.[8]

III. METHOD OF SOLUTION

For given molecular chlorine feed rate, neutral density (pressure), power, frequency, and discharge tube dimensions, the balance Eqs. (1), (2), and (4) were solved for the self-sustaining electric field, electron density, and atomic chlorine mole fraction. These equations are coupled through the dependence of the electron–particle reaction rate coefficients on the electric field and the mole fraction of atomic chlorine. The coupled system of equations was solved using the FORTRAN algorithm DERPAR.[13] The atomic chlorine density thus obtained was used as a boundary condition to solve the convective diffusion Eq. (5). The latter was solved by a finite difference method.

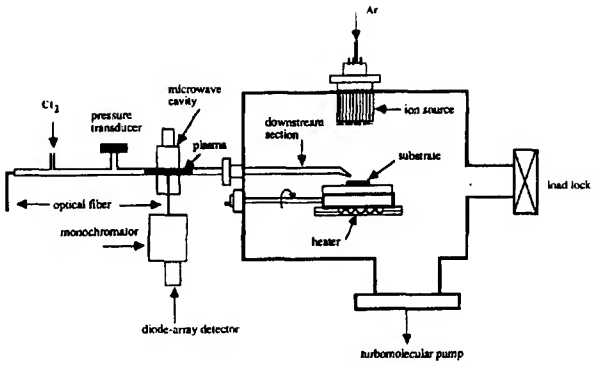

FIG. 3. Schematic of the experimental system.

IV. EXPERIMENTAL

In order to test the model predictions, etching experiments were performed in a turbomolecular-pumped ultrahigh vacuum (UHV) system (Fig. 3). Chlorine radicals were generated in a 10 mm-i.d. quartz tube using a microwave discharge operating at 2.45 GHz. The pressure in the tube was measured using a Baratron® transducer and varied with feed flow rate. The flow rate required to achieve a nominal pressure of 0.25, 0.5, and 1.0 Torr was 0.8, 2.2, and 6.0 sccm, respectively. The downstream section of the tube was 30 cm long. The tube ended with a 1.5 mm-diam nozzle and the substrate was located 1 cm away from the nozzle tip. The substrate holder was heated resistively and its temperature was controlled to within ±2 °C of the set point. Thermal contact between the substrate and the holder was achieved using silver paint. All etching experiments were carried out at a substrate temperature of 150 °C. This experimental setup is not typical of a remote plasma etching system. Nevertheless, the setup can be used to conduct well-characterized experiments to test the mathematical model predictions.

The discharge tube was pretreated with phosphoric acid in order to reduce wall recombination of atomic chlorine.[14] The tube was washed with de-ionized water and soaked in a 15% phosphoric acid solution overnight. The tube was then dried in an argon atmosphere at 250 °C. Prior to each set of experimental runs, the tube was "conditioned" by switching the plasma on for 30 min. In order to enhance reproducibility the tube was used exclusively with chlorine plasmas. It was noticed that irreproducible results were obtained when plasmas of other gases (O_2 or CF_4) were struck in the same tube.

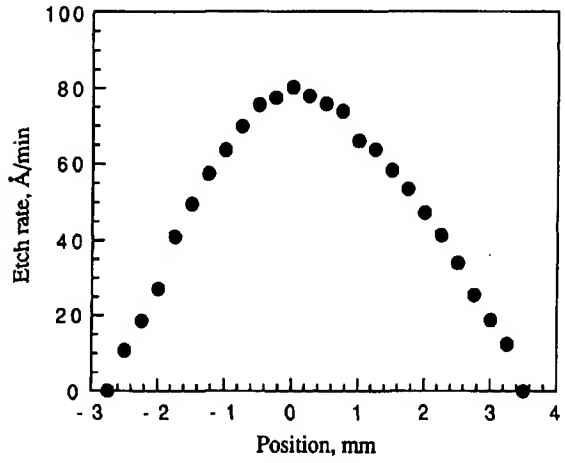

FIG. 4. Etch rate of polysilicon as a function of radius.

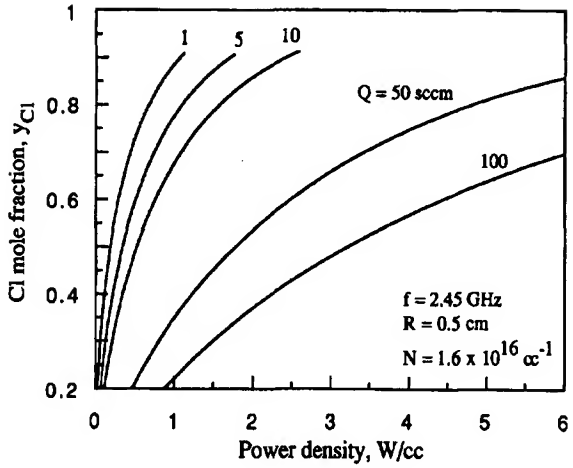

FIG. 5. Atomic chlorine mole fraction in the plasma as a function of power density, for different feed gas flow rates; $f=2.45$ GHz, $R=0.5$ cm, $N=1.6\times10^{16}$ cm^{-3}.

Heavily doped ($n^+\approx10^{20}$/cm^3 doping) polycrystalline silicon was used for etching experiments. *P*-doped polysilicon films (6000 Å thick) were deposited on 1000 Å of oxide on 6 in. wafers. Removal of the native oxide of silicon is essential to initiate Cl-atom etching. This was achieved by sputtering the native oxide with an argon ion beam extracted from a 3 cm Kaufman ion source.

The polysilicon etch rate was measured as follows: The film remaining after an etching experiment was wet etched down to the underlying oxide through a pattern of equally spaced 200 μm-wide lines. A surface profilometer (Tencor Instruments) was then used to measure the thickness of the remaining polysilicon as a function of radial position. Also, a few samples were cleaved and the cross section was examined using a scanning electron microscope (SEM) to verify the profilometer measurements. The polysilicon film etched in the form of concentric circles with the etched depth decreasing with increasing radius. Figure 4 shows a typical etch rate distribution. Based on this distribution an average etch rate was calculated. The maximum etch rate at the center was used to compare the relative etch rates between different samples.

Plasma emission was collected along the tube axis and also along a tube diameter at the center of the microwave cavity (Fig. 3). Actinometry was used to estimate the relative changes in Cl-atom density in the plasma by adding 5%–10% Ar. Argon emissions at 811.5 and 826.4 nm and Cl-atom emissions at 808.5 and 837.6 nm were monitored. Based on the emission line shapes, Gottscho and Donnely[15] concluded that the Cl 837.6 nm and Ar 826.4 nm lines may be used for actinometry provided that emission was collected from the center of the plasma away from the sheaths of their rf capacitively coupled reactor. Aydil and Economou[16] have also used actinometry to monitor the Cl-atom density in a similar reactor. In the electrodeless microwave discharge used here sheath effects are expected to be relatively unimportant.

V. RESULTS AND DISCUSSION

A. Theoretical results

1. Radical source section

Figure 5 shows the atomic chlorine mole fraction obtained in the plasma (radical source) as a function of power density for different gas feed flow rates at a constant neutral gas density. As expected, more molecular dissociation is achieved by increasing the power density delivered to the plasma. Indeed, very high degrees of dissociation are possible with only a few watts per cubic centimeter, especially at low flow rates. For a given power density, the mole fraction of atomic chlorine in the plasma decreases with increasing flow rate because the gas residence time in

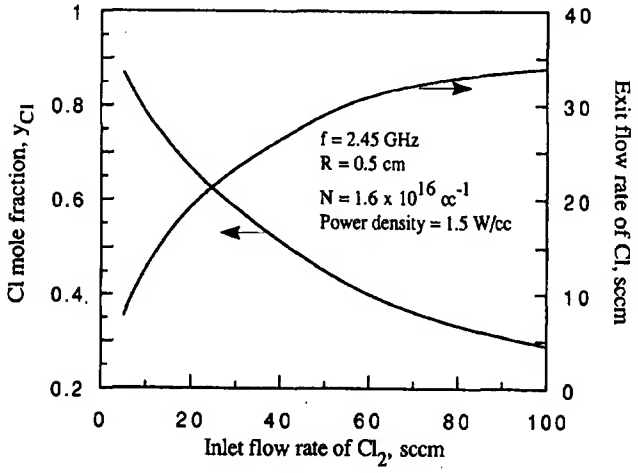

FIG. 6. Atomic chlorine mole fraction in the plasma (left axis) and flux out of the plasma (right axis) as a function of feed gas flow rate; $f=2.45$ GHz, $R=0.5$ cm, $N=1.6\times10^{16}$ cm^{-3}, and power density$=1.5$ W/cm^3.

TABLE II. Parameter values for downstream section. Values for variable quantities (e.g., N, Q_0) are representative of the experimental system.

Name	Symbol	Typical value
Volume recombination coefficient	k_v	4.5×10^{-32} cm^6/s
Wall recombination coefficient	k_{sd}	2.51 cm/s
Wall recombination probability	γ_d	2.2×10^{-4}
Cl diffusivity in Cl_2	D_{AB}	3.2×10^{18}/N cm^2/s
Gas temperature	T	350 K
Tube radius	R	0.5 cm
Length of downstream section	L_d	30 cm
Feed flow rate	Q_0	2.2 sccm
Neutral density	N	1.6×10^{16}/cm^3
Peclet number	Pe	11.76
Damköhler number (volume)	Da_v	8.81
Damköhler number (wall)	Da_w	3.84

the plasma also decreases with flow rate. Hence, the gas molecules have lower chance of dissociating as they flow through the plasma volume.

Figure 6 shows the atomic chlorine flow rate Q_{Cl} at the *plasma* exit as a function of feed flow rate of molecular chlorine. Q_{Cl} was found using the relation

$$Q_{Cl}=\frac{2y_{Cl}}{2-y_{Cl}}Q_0, \tag{10}$$

where Q_0 is the feed (Cl_2) flow rate. Equation (10) indicates that if complete dissociation is achieved in the plasma ($y_{Cl}=1$) the flow rate of atomic chlorine is twice that of the feed gas. Figure 6 shows that the atom flux *increases* with feed gas flow rate despite the fact that the degree of gas dissociation *decreases* with flow rate. A parametric investigation of the radical source region was reported elsewhere.[7] Also, results on the eedf at 2.45 GHz and 13.56 MHz have been reported before.[7,11]

2. Downstream section

We now turn our attention to the downstream section. For a constant gas temperature, there are six variables that influence the atom density and its distribution in the downstream section. These are tube radius R, length of downstream section L_d, gas flow rate Q_0, number density N, wall recombination probability γ_d (or k_{sd}), and volume recombination coefficient k_v. In addition, the atom mole fraction at the source exit has to be specified. By expressing the convective diffusion equation in dimensionless form as shown in Eq. (5), the number of parameters is reduced to three, i.e., Peclet number Pe, and Damköhler numbers for volume recombination Da_v, and wall recombination Da_w. Parameter values typical of our experimental system are shown in Table II.

Figures 7–9 show the atomic chlorine mole fraction at the exit of the downstream section as a function of Da_w for different values of Da_v. Figures 7, 8, and 9 were calculated

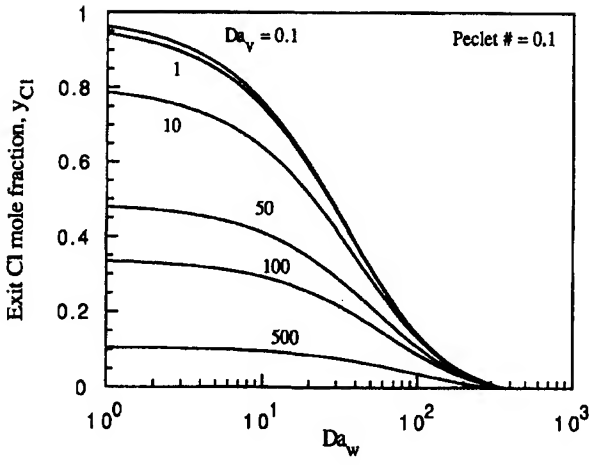

FIG. 7. Atomic chlorine mole fraction at the exit of the downstream section as a function of Da_w for different values of Da_v; Pe=0.1.

for Pe=0.1, 1, and 10, respectively, assuming complete dissociation in the plasma (i.e., $y_{Cl,0}=1$). For given tube dimensions and operating conditions one can obtain an estimate of the degree of depletion of radicals in the downstream section by utilizing these figures. The behavior of the system can be understood better if one rewrites the dimensionless groups in terms of a characteristic gas residence time τ_R,

$$\mathrm{Pe}=\frac{L_d^2}{D_{AB}\tau_R},\quad \mathrm{Da}_v=2k_vN^2\tau_R,\quad \mathrm{Da}_w=\frac{2k_s\tau_R}{R}, \tag{11}$$

where

$$\tau_R=\frac{\pi R^2NL_d}{4.48\times10^{17}Q_0}.$$

Then for a given residence time, Pe is increased by increasing L_d and/or decreasing D_{AB}. Da_v is increased by increasing k_v or gas density; and Da_w is increased by in-

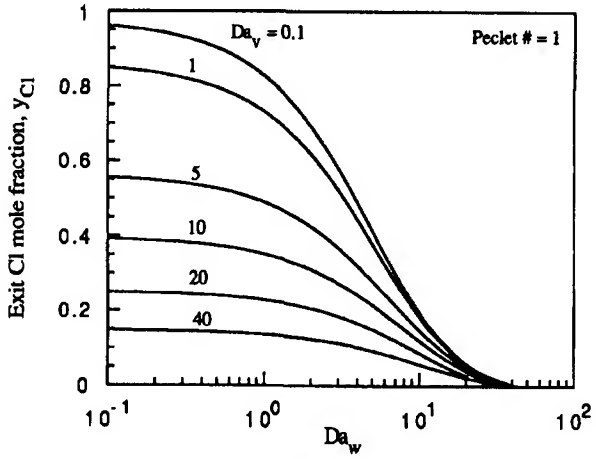

FIG. 8. Atomic chlorine mole fraction at the exit of the downstream section as a function of Da_w for different values of Da_v; Pe=1.

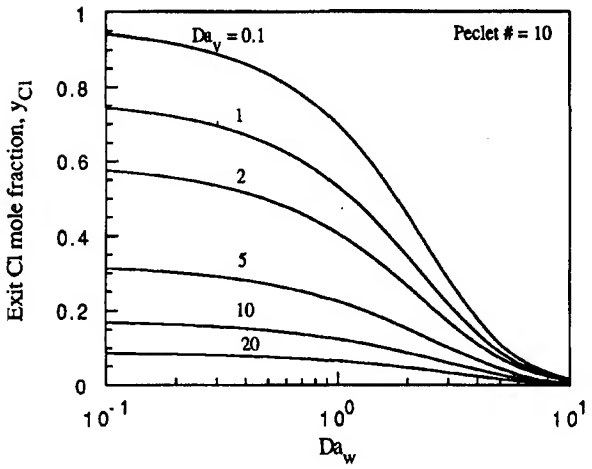

FIG. 9. Atomic chlorine mole fraction at the exit of the downstream section as a function of Da_w for different values of Da_v; Pe = 10.

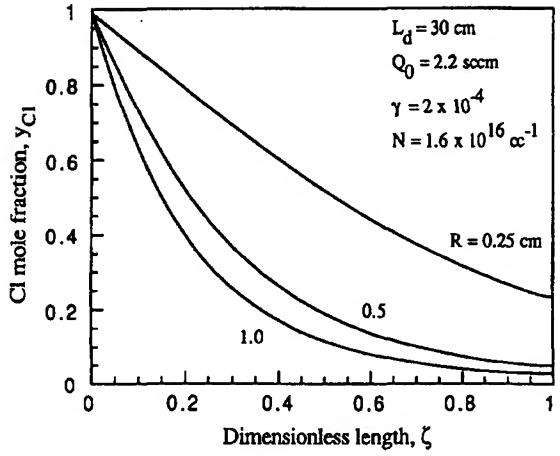

FIG. 10. Atomic chlorine mole fraction as a function of dimensionless position in the downstream section, for different values of tube radius; $N = 1.6 \times 10^{16}$ cm^{-3}, $\gamma = 2 \times 10^{-4}$, $Q_0 = 2.2$ sccm, $L_d = 30$ cm.

creasing k_s and/or decreasing R. The actual gas residence time is shorter than τ_R since the latter is based on the undissociated gas flow Q_0. The actual gas residence time can be as short as $\tau_R/2$ at complete dissociation in the plasma and without any radical decay in the downstream region.

For low values of Da_w (<0.1), the mole fraction of radicals at the tube exit $y_{Cl,e}$ is independent of Da_w. Under these conditions wall recombination is not an important loss of atomic chlorine. As Da_w increases the exit mole fraction drops, and at high Da_w there is severe depletion of radicals as they flow downstream. For low Pe, volume recombination is unimportant for values of Da_v less than 0.1. The effect of wall and volume recombination is much more pronounced for higher values of Pe (long tubes), i.e., for higher values of Pe, $y_{Cl,e}$ decreases faster with increasing either Da_w or Da_v. Figures 7–9 may also be used as design guidelines for selecting reactor dimensions and operating conditions to minimize depletion of radicals in the downstream section.

Results in terms of dimensional quantities are shown next. In the next two figures, the atom mole fraction at the inlet to the downstream section was taken as 0.99, i.e., nearly complete dissociation. Figure 10 shows the atom mole fraction as a function of position in the downstream section of the tube for different tube radii, R. Atoms decay faster with increasing tube radius. Under these conditions wall recombination is not an important atom loss mechanism, i.e., one operates in the nearly flat region of the curves shown in Figs. 7–9 (low Da_w). As R decreases however, the gas residence time in the downstream section also decreases (note that N and L_d are kept constant) and the chance for volume recombination is lower. Hence, a higher atom density is obtained at the exit. The opposite trend was observed for the radical source; the atom density increased with increasing tube radius.[7]

Figure 11 underscores the dramatic effect of pressure. By quadrupling pressure (from 0.25 to 1 Torr, nominal) the atom flux at the exit is reduced by a factor of 56 (from 0.672 to 0.012). Again, volume recombination is very significant even for pressures less than 1 Torr for the system studied. In order to counterbalance the strong pressure effect, one would need to use high gas flow rate to reduce the residence time in the downstream section (or use a short downstream section).

B. Experimental results and comparison with theory

Figure 12 shows the emission intensity of the Ar 811.5 nm and the Cl 808.5 nm lines as a function of applied power at a pressure of 0.25 Torr. The ratio of the two lines is also shown and this ratio is taken to be proportional to the Cl-atom concentration, [Cl]. It can be seen that [Cl] increases with power and saturates at high enough power. This saturation suggests that complete dissociation of molecular chlorine has been achieved (see also, Fig. 5). Fur-

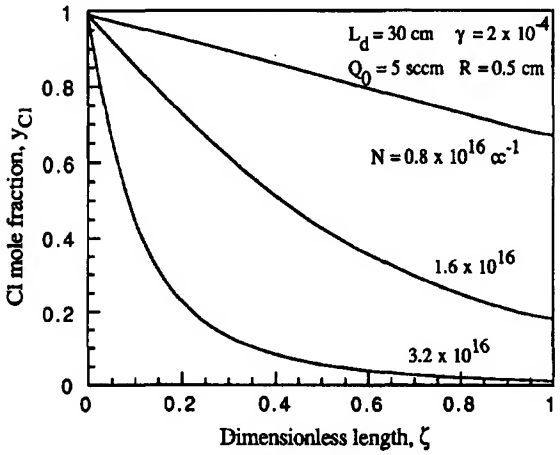

FIG. 11. Atomic chlorine mole fraction as a function of dimensionless position in the downstream section, for different values of neutral number density; $R = 0.5$ cm, $\gamma = 2 \times 10^{-4}$, $Q_0 = 5$ sccm, $L_d = 30$ cm.

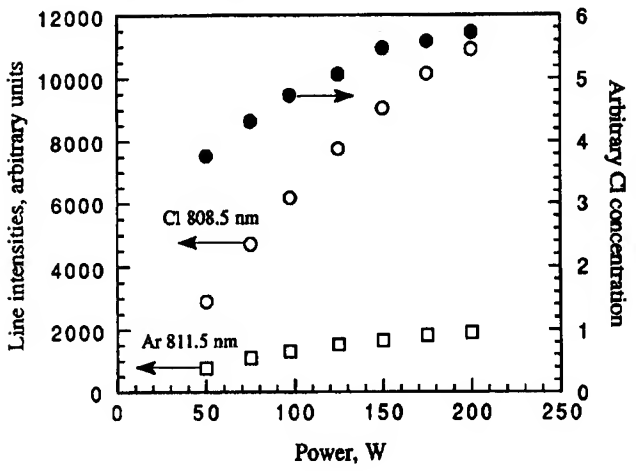

FIG. 12. Measured emission intensities of the Ar 811.5 nm and the Cl 808.5 nm lines (left axis) and Cl concentration (right axis) as a function of power; p=0.25 Torr, Q_0=0.8 sccm, R=0.5 cm.

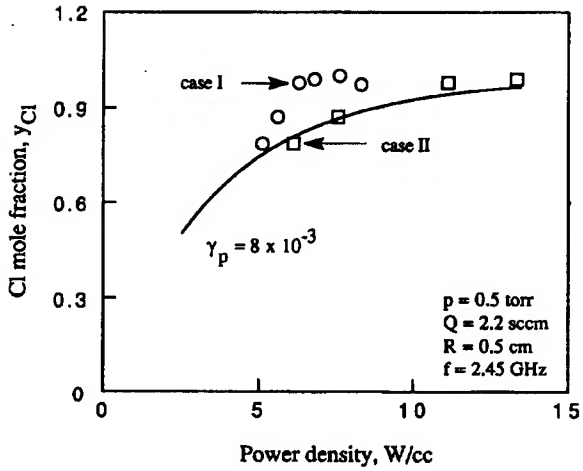

FIG. 14. Comparison between measured (points) and calculated (solid curve) Cl-atom mole fraction as a function of power density; p=0.5 Torr, Q_0=2.2 sccm, R=0.5 cm.

ther evidence of complete dissociation was the fact that the polysilicon etch rate also saturated with power (see below).

The plasma volume does not remain constant as pressure and power are varied. At low pressure and/or high power the length of the plasma column extends beyond the edges of the 4.3 cm-long microwave cavity. In order to calculate the power density, two extreme cases were used. In case I, the power density was calculated by dividing the input power by the volume physically occupied by the plasma (plasma column length×tube cross sectional area). In case II, the input power was divided by the volume occupied by the plasma at the minimum power at which the plasma could be sustained for a given pressure. It should be noted that the plasma intensity was not uniform along the plasma column. Therefore, the power density represents an average value.

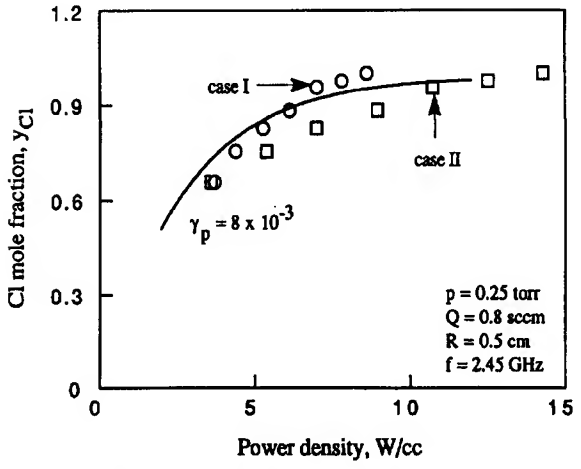

FIG. 13. Comparison between measured (points) and calculated (solid curve) Cl-atom mole fraction as a function of power density; p=0.25 Torr, Q_0=0.8 sccm, R=0.5 cm.

Figures 13 and 14 show a comparison between measured and calculated Cl-atom mole fraction. The wall recombination probability was used as the only fitting parameter. Curves I and II correspond to cases I and II, respectively, for calculating the power density. By choosing a value of $\gamma_p = 8 \times 10^{-3}$ the agreement between theory and experiment is satisfactory. Ogryzlo[14] has reported a wall recombination probability of 4×10^{-5} for chlorine atoms on quartz poisoned with phosphoric acid. However, the tube walls are modified when exposed to the plasma.

Atom flux at tube exit: The Cl atom flux at the reactor exit was calculated from the measured polysilicon etch rate using the known reaction kinetics for this system. The center etch rate is shown in Table III as a function of power. The etch rate does saturate at high power indicating complete dissociation in the plasma. Ogryzlo *et al.*[17] reported the following expression for etch rate of poly with Cl atoms

$$ER(\text{Å/min}) = \gamma_0 n_{Cl} T^{0.5} \exp(-E/RT) N_d^{\alpha}, \qquad (12)$$

where α=0.39, $\gamma_0 = 4.04 \times 10^{-18}$, E=4.7 kcal/mol is the activation energy, n_{Cl} is the Cl-atom density, and N_d is the dopant density. For the system at hand the etch rate is calculated to be 625 Å/min/mTorr of atomic chlorine.

Based on an average etch rate of 74 Å/min for 150 W and 0.25 Torr (Table III), the atom flux at the substrate is

TABLE III. Measured etch rate at center. Average etch rate is shown in parenthesis.

Power (W)	Etch rate (Å/min) 0.25 Torr	0.5 Torr
60	110	110
90	175	116
120	193	131
150	182 (74)	147 (61)

TABLE IV. Predicted and measured exit Cl mole fraction.

Pressure (Torr)	Feed flow rate (sccm)	Cl mole fraction at exit	
		Measured	Predicted
0.25	0.8	0.083	0.082
0.50	2.2	0.025	0.037
1.0	6.0	0.015	0.014

calculated to be $4.76\times10^{16}/cm^2$ s. For an etched diameter of 9 mm, this corresponds to a mass flow rate of 3×10^{16}/s or $Q_{Cl}=0.067$ sccm of atomic chlorine. For 0.25 mTorr, the feed gas flow rate was $Q_0=0.8$ sccm. Using Eq. (10), the exit Cl mole fraction is 0.083, a drastic drop compared to the value of unity at the inlet of the downstream section. This drop is a result of the long downstream section of the tube. Similar experiments were performed for 0.5 and 1.0 Torr, and the results are summarized in Table IV. The predicted Cl atom mole fractions at the tube exit are also shown in this table. Again, the wall recombination probability γ_d was the only fitting parameter and it was found to be 2.2×10^{-4}. The value of γ is different for the source and downstream regions. This is not surprising since exposure to the plasma modifies the treated quartz surface in the source region. That the surfaces of the source and downstream regions are different can even be observed visually.

For high values of wall recombination probability, wall recombination will become diffusion controlled and radical concentration gradients along the radial direction will be established as well. The transition from reaction- to diffusion-controlled regime may be estimated by setting the Thiele modulus $\Phi=1$,

$$\Phi=\left(\frac{2k_{sd}R}{D_{AB}}\right)^{1/2}. \tag{13}$$

For 0.25 Torr and $R=0.5$ cm, Φ becomes unity for a wall recombination probability of $\gamma_d=3.5\times10^{-2}$. Since for the present system $\gamma_d=2.2\times10^{-4}$, Φ is less than unity and it is reasonable to neglect any radial concentration gradients in Eq. (5). Also, the mean-free-path for atomic chlorine in a 50:50 mixture of Cl and Cl_2 at 0.25 Torr was estimated to be 0.2 mm.[18] This gives a Knudsen number of $2R/\lambda=10/0.2=50$. Thus, the assumption of viscous flow at 0.25 Torr pressure is also reasonable.

VI. SUMMARY AND CONCLUSIONS

A combined theoretical–experimental investigation of a remote plasma etching reactor has been presented. The chlorine plasma etching of polysilicon was taken as a model system for analysis. However, the same methodology can be applied to other systems as well. Separate models for the radical source and downstream sections were developed based on fundamental principles. A parametric investigation was carried out to assess the effect of reactor dimensions and operating conditions on the radical density in the plasma and the radical flux at the reactor exit. The results may be summarized as follows.

(1) Long downstream section is detrimental irrespective of other process parameters.

(2) The gas residence time in the downstream section should be made as small as possible. This can be achieved by using high flow rate, or using a small tube radius, or using a short downstream section. A small tube radius in the downstream section is especially effective when the wall recombination probability is low. Quantitative estimates can be made using Figs. 7–9. However, sufficient residence time should be allowed in the plasma (radical source) section, so as to enhance gas dissociation. This can be achieved by using a larger tube radius in this section. A compromise could be reached by using a tube with different radius for the plasma and downstream sections.

(3) High pressures in the downstream section are detrimental for chlorine atoms, since volume recombination increases rapidly will pressure.

(4) Operating at high flow rates is advantageous since the radical flux out of the plasma is higher and the Cl-atom loss in the downstream section is minimized.

The extent of dissociation in the plasma was monitored using actinometry. Saturation of atom density as a function of applied power was indicative of complete gas dissociation in the plasma. By using the wall recombination probability γ_p as the only adjustable parameter, good agreement between predicted and measured Cl atom density in the plasma was obtained.

Based on the measured etch rate of polysilicon and the known reaction kinetics the radical flux at the tube exit was determined. Again, using the wall recombination probability γ_d as the only adjustable parameter, the measured flux at the exit matched calculated values.

From a practical standpoint, the analysis presented here can provide guidelines for the design and operation of remote plasma reactors. Including more complicated chemistry in the model is straightforward. However, it was felt that the basic chemistry used for the chlorine system provides a satisfactory description of that system. For reactors with short downstream section, the present model needs to be extended to include charged particle kinetics and gas temperature profiles.

ACKNOWLEDGMENTS

This work was supported by the State of Texas through the Texas Center for Superconductivity at the University of Houston and the Advanced Technology Program. The authors are grateful to Dr. J. Wolfe of the Electrical Engineering department for many helpful discussions on the design of the experimental apparatus. Thanks are due to Dr. Lee Lowenstein of Texas Instruments Inc. for providing the silicon wafers.

[1]J. Kuo, M. Hong, D. J. Trevor, R. M. Flemming, A. E. White, R. C. Farrow, A. R. Kortran, and K. T. Short, Appl. Phys. Lett. 53, 2683 (1988).
[2]S. Sugata, A. Takamori, N. Takado, K. Asakawa, E. Miyauchi, and H. Hashimoto, J. Vac. Sci. Technol. B 6, 1087 (1988).
[3]G. Lucovsky, P. D. Richard, D. V. Tsu, S. Y. Lin, and R. J. Markunas, J. Vac. Sci. Technol. A 4, 681 (1986).

[4]V. Vukanovic, G. A. Takacs, E. A. Matuszak, F. D. Egitto, F. Emmi, and R. S. Horwath, J. Vac. Sci. Technol. B **6**, 66 (1988).
[5]D. Lishan and E. Hu, Appl. Phys. Lett. **56**, 1667 (1990).
[6]S. C. Deshmukh and D. J. Economou (unpublished).
[7]S. C. Deshmukh and D. J. Economou, J. Appl. Phys. **72**, 4597 (1992).
[8]M. J. Kushner, J. Appl. Phys. **71**, 4173 (1992).
[9]S.-K. Park and D. J. Economou, J. Appl. Phys. **66**, 3256 (1989).
[10]G. L. Rogoff, J. M. Kramer, and R. B. Piejak, IEEE Trans. Plasma Sci. **PS-14**, 103 (1986).
[11]E. S. Aydil and D. J. Economou, J. Electrochem. Soc. **139**, 1396 (1992).
[12]P. E. Luft, Joint Inst. for Lab. Astrophysics, Univ. of Colorado, Boulder, Report 14 (1975).
[13]M. Kubicek, ACM Trans. Math. Software **2**, 98 (1976).
[14]E. A. Ogryzlo, Can. J. Chem. **39**, 2556 (1961).
[15]R. A. Gottscho and V. M. Donneley, J. Appl. Phys. **56**, 245 (1984).
[16]E. S. Aydil and D. J. Economou, J. Electrochem. Soc. **139**, 1406 (1992).
[17]E. A. Ogryzlo, D. E. Ibbotson, D. L. Flamm, and J. A. Mucha, J. Appl. Phys. **67**, 3115 (1990).
[18]*Vacuum Manual*, edited by L. Holland, W. Steckelmacher, and J. Yarwood (SPON, London, 1974).